Composites: Part A 181 (2024) 108141

Contents lists available at ScienceDirect

Composites Part A

journal homepage: www.elsevier.com/locate/compositesa

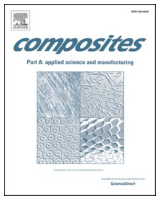

Influence of physical ageing and fibre proximity on the local mechanical response of the Elium® thermoplastic composite matrix

Sarah F. Gayot [a,b,*], Nathan Klavzer [a], Alain Guillet [c], Christian Bailly [b], Pierre Gérard [d], Thomas Pardoen [a,e], Bernard Nysten [b]

[a] Institute of Mechanics, Materials and Civil Engineering (iMMC), UCLouvain, B-1348, Louvain-la-Neuve, Belgium
[b] Institute of Condensed Matter and Nanosciences (IMCN), UCLouvain, B-1348, Louvain-la-Neuve, Belgium
[c] Plate-forme Technologique de Support en Méthodologie et Calcul Statistique (SMCS), UCLouvain, B-1348, Louvain-la-Neuve, Belgium
[d] Groupement de Recherche de Lacq, Arkema, RD 817, BP 34 64170, Lacq, France
[e] WEL Research Institute, Avenue Pasteur 6, B-1300, Wavre, Belgium

ARTICLE INFO

Keywords:
Polymer-matrix composites (PMCs)
Thermoplastic resin
Micro-mechanics
Statistical methods

ABSTRACT

The prediction of the micromechanical response of fibre-reinforced polymer composites with numerical models relies on the assumption that the matrix behaves like a bulk sample of the same polymer. Yet, the presence of fibres likely impacts the thermochemical history and mechanical behaviour of the matrix (e.g. formation of an interphase during processing). In this work, micromechanical analysis of a thermoplastic polymer matrix is performed on glass fibre-reinforced composite samples manufactured by vacuum infusion and in-situ polymerisation. The interphase thickness and mechanical behaviour are assessed by atomic force microscopy (AFM). The mechanical properties of the matrix beyond the interphase are measured by nanoindentation and AFM in intra- and inter-tow matrix pockets, for different levels of natural physical ageing. While the distance to the nearest fibre does not significantly impact the polymer properties at a given ageing time, fibre proximity affects the rate and extent of physical ageing experienced by the polymer.

1. Introduction

Multiscale mechanical models aim at predicting the failure of macroscopic components and structures by considering the deformation and failure mechanisms occurring in the material at smaller length scales. This bottom-up approach simplifies and makes more robust the structural integrity assessment of parts by drastically reducing the need for mechanical testing [1,2]. This is especially relevant for materials with high production costs such as fibre-reinforced polymer composites. In this case, modelling starts at the micrometre scale and focuses on the behaviour of a single (or a few) elemental fibre(s) embedded in a polymer matrix. The matrix is generally assumed to have the same constitutive properties as the bulk, unreinforced polymer. However, this assumption may not be realistic for two reasons. First, an interphase region has been identified experimentally for a variety of composite systems. Most of these studies relied on various mechanical modes of atomic force microscopy (AFM) [3–17], though a few authors relied on other techniques such as nanoscratch [18,19], transmission electron microscopy [20,21], dynamic nano-mechanical analysis [22], and, more recently, nanoscale digital image correlation [23]. The fibre–matrix interphase can be defined as a transition zone which behaves differently from both the polymer and fibre materials, and can extend up to a few micrometres from the fibre surface. This interphase forms as a result of the chemical reaction and/or interdiffusion phenomena occurring between the fibre sizing and the matrix material during curing. Secondly, beyond this interphase region, the polymer matrix *per se* may also differ from the unreinforced polymer in terms of thermal history, molecular structure (e.g. crosslinking density, transcristallinity, chain length and specific anisotropic chain orientation/alignment), residual stress distribution [24–30] and ageing behaviour [31].

To settle the question, the local mechanical properties of the composite matrix must be assessed in-situ and compared to the nominally similar unreinforced polymer (also referred to as “bulk” or “neat” polymer), which is technically challenging. Indentation techniques may be used, provided the mechanical response of matrix pockets can be decoupled from that of the surrounding fibres. As the polymer matrix is indented, a specific stress state - consisting of a plastic zone surrounded by an elastic region - develops under the tip, with the deformation

* Corresponding author.
E-mail address: sarah.gayot@uclouvain.be (S.F. Gayot).

https://doi.org/10.1016/j.compositesa.2024.108141
Received 7 September 2023; Received in revised form 9 January 2024; Accepted 10 March 2024
Available online 16 March 2024

decaying as the distance to the tip increases. If the indent is performed very close to the fibre–matrix interface, the development of the indentation stress field may be constrained by the nearby presence of the stiffer fibre material. This can lead the measured indentation modulus and hardness values to be overestimated with respect to reality [4,6,8,17,18,24–26,29,32,33]. A few authors compared the mechanical response of a polymer composite matrix to those of the unreinforced polymer using instrumented indentation experiments and finite element (FE) simulations [15,17,24–26,34–37]. The pioneering study by Gregory and Spearing [24] focused on an epoxy resin and on the corresponding carbon fibre prepreg laminate. Nanoindentation was used in the continuous stiffness measurement (CSM) mode to measure the elastic modulus and hardness of resin pockets in the composite, as a function of penetration depth h. A 2D-axisymmetric FE model of the experiment was designed as follows. A rigid conical punch was pushed into a matrix pocket of radius x, approximated by a cylinder, and whose external surface was subjected to rigid ("built in") boundary conditions to simulate the fibre constraining effect. Modulus (and hardness) values obtained from nanoindentation simulations were found to be unconstrained in the cases where $x/h > 25$. By applying this simple geometric criterion to experimental nanoindentation data, the modulus and hardness of the unconstrained epoxy resin were found to be up to 30 % larger in the composite. However, the minimum indentation depth in this work was equal to 500 nm, meaning that matrix pockets with a radius $x < 12.5$ μm could not be characterised. More recently, Hardiman et al. [25] performed a similar study on another epoxy/carbon fibre prepreg system. Lower indentation depths (down to 100 nm) were imposed, which allowed characterising smaller resin pockets. The modulus and hardness values of the unconstrained composite matrix were found to be up to 20 % higher than in the bulk resin for $x < 15$ μm. No significant difference was observed between the two systems for $x > 15$ μm. Another study focusing on the mechanical properties of a composite polymer matrix versus the unreinforced polymer was recently presented by Pecora et al. [29] following a slightly different approach. A 3D-architectured carbon fibre/epoxy composite system was produced by liquid moulding instead of prepreg consolidation, leading to the presence of inter-tow matrix pockets with an average radius of hundreds of micrometres. The elastic and time-dependent mechanical properties of the bulk resin were compared to those of the inter-tow composite resin pockets via cyclic nanoindentation testing. An additional distinction was made between resin pockets located at the surface of the composite specimen versus the ones found in the "core" of the sample. The results showed a small (in the order of a few %) but significant difference in elastic and viscoelastic properties between the three conditions (composite surface, composite core and unreinforced polymer). The properties of the composite core matrix were closer to the unreinforced polymer than to the surface composite matrix, which was attributed to differences in thermal history across the thickness of the plate during processing.

Yet, none of the three aforementioned studies considered the additional impact of physical ageing on the mechanical response of both the fibre-reinforced and unreinforced polymer specimens. Amorphous solids, including glassy polymers, are not thermodynamically stable: when cooled down from the liquid (or rubbery) state to a temperature T_1 below the glass transition temperature T_g and maintained at this temperature for a period of time Δt, they undergo structural changes associated to a decrease in the mobility of the macromolecular chains as they enter a configuration with lower excess energy (which can be assimilated to a decrease of the free volume). This phenomenon is referred to as physical ageing, whose rate increases as the ageing temperature T_1 increases closer to T_g [38]. Physical ageing may, among others, impact the mechanical properties of glassy polymers (in particular the quasi-static properties, fracture toughness and viscoelastic/viscoplastic behaviour), which can be detrimental to the long-term performances [38,39]. Contrary to other ageing phenomena, in particular chemical ageing, physical ageing is completely reversible upon heating the material above T_g. The consequences of physical ageing on the mechanical properties of glassy polymers and on their composites have been extensively studied [31,40–45]. A few authors, in particular the team of Cangialosi, showed that the addition of reinforcements into polymer glasses could, in some cases, accelerate the physical ageing by favouring the diffusion of free volume outside of the system [46–48]. To our knowledge, however, the influence of reinforcement proximity on the rate and extent of physical ageing experienced locally by glassy polymers has not yet been explored from a micro- or nanomechanical point of view. Acknowledging and accounting for this phenomenon is crucial for interpreting any observed difference in mechanical properties between a polymer composite matrix and the equivalent unreinforced polymer.

In this study, the local mechanical response of a thermoplastic methacrylic composite matrix is compared to the unreinforced polymer. The objective is to determine in situ the dual influence of fibre proximity and physical ageing on the polymer properties. To achieve this goal, micro- and nanomechanical analyses of a methacrylic thermoplastic resin are performed via nanoindentation and AFM. In particular, the properties of the unreinforced resin are compared to those of the inter- and intra-tow matrix pockets of a glass fibre-reinforced composite made of the same resin. The unreinforced resin and composite specimens are subjected to a thermal rejuvenation treatment above T_g, in order to reset the reference t_0 of the ageing time. A first set of nanoindentation measurements is acquired at $t = t_0$, and the experiment is repeated at t_3, t_5 and t_{17}, i.e. after 3, 5 and 17 months of "natural" physical ageing (i.e. ageing under ambient conditions), respectively. A second thermal rejuvenation treatment is applied to the polymer and composite specimens after 18 months, resetting again the ageing time to 0. The final set of nanoindentation measurements is obtained at that moment, which is referred to as t_0'. The validity of the $x/h > 25$ criterion, established by Gregory and Spearing [24], is assessed in the case of interest using FE simulation of the nanoindentation experiment. A comprehensive statistical comparison of the nanoindentation results is performed to explore the mixed influence of (1) fibre proximity and (2) level of physical ageing on the resin's modulus and hardness values. Additional AFM analyses are carried out in intra- and inter-tow composite matrix pockets at t_0 and t_5, and the measured modulus values are confronted to the corresponding nanoindentation results. In parallel, AFM is also used for measuring the thickness and modulus of the fibre–matrix interphase region of the composite material. The final objective of this in-depth investigation is to determine to which extent the in-situ local mechanical response of a methacrylic polymer matrix in between fibres differs from that of the bulk polymer. Unlike previous studies on the topic [24,25,29], this work also considers the impact of time on the observed differences, through the concept of physical ageing. The practical interest of such a fundamental study may not be evident at first, from a composite manufacturer's viewpoint. However, understanding the long-term ageing behaviour of fibre-reinforced composites is essential for accurately predicting the evolution of composite performances over the course of their service life – which is the ultimate purpose of this work.

2. Theoretical background

2.1. Instrumented indentation techniques [49]

Indentation testing consists in pushing a rigid tip of known geometry into a flat material surface to determine its mechanical properties. The measurement of the contact area between the indenter and the material during the test enables the extraction of, e.g., the indentation modulus and hardness of the test material using contact mechanics models. Particularly, instrumented indentation techniques (IITs) rely on the indirect estimation of the contact area from force-displacement curves recording the load P applied to the indenter as a function of the penetration depth h of the indenter. Several versions of IITs exist, depending on the order of magnitude of the tip apex radius R, the applied load P or

the penetration depth h involved. In this work, both nanoindentation ($R \sim 100$ nm, $P_{max} \sim 10$ mN, $h \sim 1$ μm) and nanomechanical AFM ($R \sim 10$ nm, $P_{max} \sim 0.1$ mN, $h \sim 1$ to 10 nm) measurements were performed, resulting in probed volumes in the μm^3 and nm^3 ranges, respectively.

2.2. Nanoindentation

Nanoindentation has been extensively used since the 2000s to determine the indentation hardness H and reduced indentation modulus E^* of materials, which are given by

$$H = \frac{P}{A_c}, \tag{1}$$

$$E^* = \frac{\sqrt{\pi}}{2}\frac{S}{\sqrt{A_c}}, \tag{2}$$

where A_c is the projected contact area between the tip and the sample, and $S = dP/dh$ is the unloading contact stiffness. E^* is the reduced indentation modulus related to the elastic moduli E_m and E_p and Poisson ratios ν_m and ν_p of the test and indentation tip materials, respectively:

$$\frac{1}{E^*} = \frac{1-\nu_m^2}{E_m} + \frac{1-\nu_p^2}{E_p}. \tag{3}$$

In the case of measurements on polymer materials, the tip can be considered as infinitely rigid and the reduced elastic modulus only depends on the polymer modulus and Poisson ratio. The polynomial function relating A_c to the contact depth h_c can be obtained through calibration. The common theoretical approach to extract E and H from load-displacement curves relies on the Oliver and Pharr model [50], which assumes sink-in of the indented material under the tip. The contact depth h_c depends on the penetration depth h via

$$h_c = h - \varepsilon\frac{P}{S}, \tag{4}$$

where ε is a constant describing the indenter geometry. Today, most nanoindentation tests rely on the continuous stiffness measurement (CSM) mode, which enables the continuous monitoring of contact stiffness as a function of indentation depth h by superposing a small-amplitude cyclic displacement to the "static" displacement [50].

2.3. Nanomechanical mapping with AFM

The PeakForce Tapping® mode with quantitative nanomechanical mapping (PFT-QNM) of AFM [51] allows quantitative mechanical mapping of a surface at the micro- and nano-scales, while also providing topological data. In this mode, the probe is imposed an off-resonance vertical cyclic displacement of a few tens of nanometres at a frequency typically in the kHz range, leading the probe tip to indent the specimen surface periodically. A load (P) versus penetration depth (h) curve is acquired during each "approach-indentation-retraction" cycle, from which various parameters/properties can be extracted such as the maximum indentation depth, the tip-surface adhesion force, the elastic modulus and the energy dissipation. The Derjaguin, Muller and Toporov (DMT) model [52] is often used for modulus calculation, assuming the AFM tip is infinitely rigid with a spherical apex of radius R. In this case, the relationships between the load applied by the probe, P, the radius of the contact area, a, and the tip penetration depth, h, are the following:

$$a^3 = \frac{3}{4}\frac{R}{E^*}(P + F_{adh}), \tag{5}$$

$$h = \frac{a^2}{R}, \tag{6}$$

$$P = \frac{4}{3}E^*\sqrt{R}h^{3/2} - F_{adh}, \tag{7}$$

where F_{adh} is the adhesion force due to Van der Waals tip-surface interactions.

In AFM-based nanomechanical techniques, the tip penetration depth, h, is indirectly obtained as the difference between the vertical displacement z imposed to the probe (or the sample), and the cantilever vertical deflection d:

$$h = z - d. \tag{8}$$

This imposes a careful selection of the AFM probe as a function of the mechanical properties of the analysed material. In particular, the cantilever stiffness, k_c, should be of the same order of magnitude as the contact stiffness k_N [53], which is expressed as

$$k_N = \frac{dP}{dh} = 2aE^* = 2E^*\sqrt{R}h. \tag{9}$$

If $k_N \gg k_c$, i.e. if the cantilever is too compliant with respect to the contact stiffness, the probe hardly indents the surface. In this case, the cantilever deflection, d, is almost equal to the vertical displacement, z, and the penetration depth, h, is computed as the difference of two large numbers resulting in a small value with a large uncertainty. If $k_N \ll k_c$, the cantilever deflection values are small with respect to the photodetector limit of detection, leading to low signal-to-noise ratio.

The absolute values of the modulus obtained in PFT-QNM imaging should be considered with caution for several reasons, see e.g. [5,54–56]. First, errors in the characterisation of tip radius and cantilever stiffness values (during PFT-QNM calibration) impact the accuracy of modulus calculations by up to 5 and 10–20 %, respectively [5,53,57]. Probe wear during calibration itself and/or during specimen imaging is also commonly observed [53,54], adding up to the uncertainty on tip radius value. Additionally, surface roughness may interfere with the definition of the contact point and contact radius in two cases: (1) if the root-mean-square roughness value is close to that of indentation depth [54] and/or (2) if abrupt slope changes occur [6,14,58]. Phenomena related to the viscoelastic and viscoplastic nature of polymeric materials like Elium (i.e. creep, dependency on the loading rate) are another well-known source of error [54,57,59,60]. Misestimation of the specimen's Poisson ratio prior to the AFM experiment may also interfere with modulus calculation, as shown by eq. (2) [57]. Consequently, modulus absolute values obtained by PFT-QNM are strictly comparable only for data obtained under the same experimental conditions (same probe, same calibration and operating parameters).

2.4. Linear mixed models and confidence intervals in statistics [61]

Materials scientists often rely on statistical modelling to assess the influence of one (or several) parameter(s), known as "fixed effects", on a response variable of interest. Common statistical tests such as correlation tests, t-tests or ANOVA derive from linear regression models, whose applications are restricted to the analysis of fully independent datasets. But one individual may provide multiple observations and/or several individuals can be somehow related (e.g. from the same family), which can introduce bias into the data. One way to artificially restore independence is through the averaging of related data points, which results in a significant loss of information. The preferred solution is to rely on linear mixed models instead of linear models. Linear mixed models can account for non-independent data via "random effects", i.e. grouping variables which are known to influence the response alongside the fixed effects. In other words, there are as many fitted models as there are groups of interdependent data. Random-intercept mixed models assume the influence of the fixed effect(s) on the response variable to be the same for each group of data, but allows differences in baseline values between groups. Consequently, all fitted models share the same slope, while intercept values can change. Such models are expressed as:

$$\text{Response variable} \sim \text{Fixed effect} + (1|\text{Random effect}). \tag{10}$$

Table 1
Nomenclature used for describing temporal measurement conditions (i.e. ageing time).

Type of condition	Temporal (i.e. WHEN measurements were performed)				
Notation in text/figures	t_0	t_3	t_5	t_{17}	t_0'
Level of physical ageing x (months)	0	3	5	17	0
Treatment(s) experienced by specimen	thermal rejuvenation	thermal rejuv. followed by x months of natural ageing ($t_x = t_0 + x$)			thermal rejuv., 18 months of ageing and 2nd thermal rejuv.

3. Materials and methods

3.1. Materials

The liquid resin used for producing the bulk and fibre-reinforced polymer specimens comprised a methyl methacrylate-based monomer formula, Elium® 191O/SA[1] (Arkema, France) with a peroxide thermal initiator (Luperox® K10, Arkema, France). The composite preform was made from quasi-unidirectional (UD) non-crimp glass fabric plies from Chomarat (France) with an areal weight of 1.03 kg.m^{-2} (85 % warp and 15 % weft). Consumables for composite bagging and infusion were obtained from Diatex SAS (France).

3.2. Preparation of the polymer and composite specimens

3.2.1. Manufacturing of composite specimens

A composite plate was manufactured by vacuum infusion of a 90-ply pseudo-UD glass fabric layup. The resin mix was prepared by combining three parts initiator for one hundred parts monomer formula under mechanical stirring. The mixture was degassed for 1 min at 50 mbar and infused at a pressure close to 60 mbar, parallel to the fibre tow orientation. The resin was left to polymerise within the preform after clamping shut the resin inlet and vacuum line. No external heating was applied during the process. The final part had a total thickness of 73 mm and a fibre volume fraction close to 0.5. Cubic specimens of dimensions $10 \times 10 \times 10$ mm^3 were extracted from the core of the plate, according to the sectioning diagram presented in the Supplementary Information.

3.2.2. Manufacturing of resin specimens

A degassed resin mix was prepared as described previously, casted into a Ø 14 mm borosilicate glass test tube coated with release agent Chemlease 41–90 (Chem-Trend GmbH, Germany), and left to polymerise at room temperature. After cooling, the resin sample was removed from the mould. The first few centimetres below the resin/air interface were cut off and discarded, as peroxide initiators are sensitive to air inhibition. Cylinders with height and diameter both equal to 12 mm were lathed from the remainder of the resin sample.

3.2.3. Thermal rejuvenation and physical ageing

Prior to mechanical testing, the bulk polymer and composite specimens were subjected to thermal rejuvenation through heating at a temperature T_0 slightly above their glass transition temperature T_g until thermodynamic equilibrium is achieved, and then quenching down to a temperature T_1 below T_g as described by Struik [38]. The purpose of a thermal rejuvenation treatment is twofold: (1) relaxing any internal stresses and preferential chain orientations induced by processing and (2) "resetting" the amount of free volume. In practice, the specimens were placed in a laboratory furnace preheated at 100 °C (i.e. 3 degrees above the T_g value of Elium 191O/SA as measured by [62]), held at this temperature for 10 min, then taken out and left to cool down to room temperature, i.e. close to 20 °C. The duration of the heating step (i.e. 10 min) was selected to ensure homogenous heating of the specimens up to 100 °C (as verified by solving the heat equation). The time of the quench, referred to as t_0, was considered as the origin of the ageing time [38,39] for the measurements performed at t_3, t_5 and t_{17} (i.e. 3, 5 and 17 months). A second, similar thermal rejuvenation treatment was applied to the specimens at $t_0' \approx t_0 + 18$ months, resetting again the origin of the ageing time to zero. The nomenclature used for describing the "ageing status" of the specimens upon mechanical testing (i.e. t_0, t_3, t_5, t_{17} and t_0') is summarised in Table 1. Differential scanning calorimetry (DSC) experiments were conducted in order to confirm the occurrence of physical ageing in Elium under ambient conditions, see section 3 of the Supplementary Information.

3.2.4. Polishing of composite and bulk specimens

Immediately after each rejuvenation treatment (i.e. around t_0 and t_0'), all specimens were polished as described in the Supplementary Information.

3.3. Micromechanical characterisation by nanoindentation and AFM

3.3.1. Definition of measurement conditions

Fig. 1 shows a micrograph of the polished surface of a glass fibre-reinforced Elium composite specimen. As mentioned in the introduction, the quasi-UD architecture of the reinforcing fabric gives rise to two categories of matrix pockets in the composite material: (1) intra-tow pockets, whose smallest dimension does not exceed a few microns (up to a maximum of 20 μm), and (2) inter-tow pockets, which are more than ten times larger as illustrated by Fig. 1. The unreinforced resin is referred to as condition (3), so that the measurement conditions are numbered in the order of the average distance to the closest fibre (unreinforced resin can be considered as an infinitely large matrix pocket). As a reminder for the reader, a description of each measurement condition (1), (2) and (3) is presented in Table 2.

3.3.2. Nanoindentation

The nanoindentation measurements were performed with an Agilent G200 device equipped with a Berkovich diamond tip and a Dynamic Contact Module (DCM II) head. The CSM mode was used at a frequency of 75 Hz and with a harmonic displacement value of 1 nm. The maximum penetration depth h_{max} was set to 500 nm, while the strain rate target was equal to 0.05 s^{-1}. Indentation modulus E and hardness H values were directly calculated from raw data by the KLA NanoSuite software (version 6.54.0) via the Oliver and Pharr method [50]. E and H datasets were acquired for conditions (1), (2) and (3) (cf. Table 2) at each of the following ageing times: t_0, t_3, t_5, t_{17} and t_0' (cf. Table 1). For each indent performed in condition (1), the distance x between the centre of the residual imprint and the nearest glass fibre was measured from optical micrographs via the open-source software ImageJ [63].

3.3.3. AFM

AFM indentation experiments were carried out on a Dimension Icon and a MultiMode 8 systems (both from Bruker Corp., USA), using the PeakForce Tapping® mode with quantitative nanomechanical mapping (PFT-QNM) mode [51]. The built-in tool of the Nanoscope operating software was used for extracting modulus values from the raw AFM data, via the DMT model [52] described previously. RTESPA-300 and TESPA-

[1] Elium® 191O/SA has been formulated to meet the requirements of infusion processes requiring large open times. It is able to polymerise under ambient conditions, i.e. without the need for external heating. The main material properties of Elium® 191O/SA are summarised in Table S1 of the Supplementary Information.

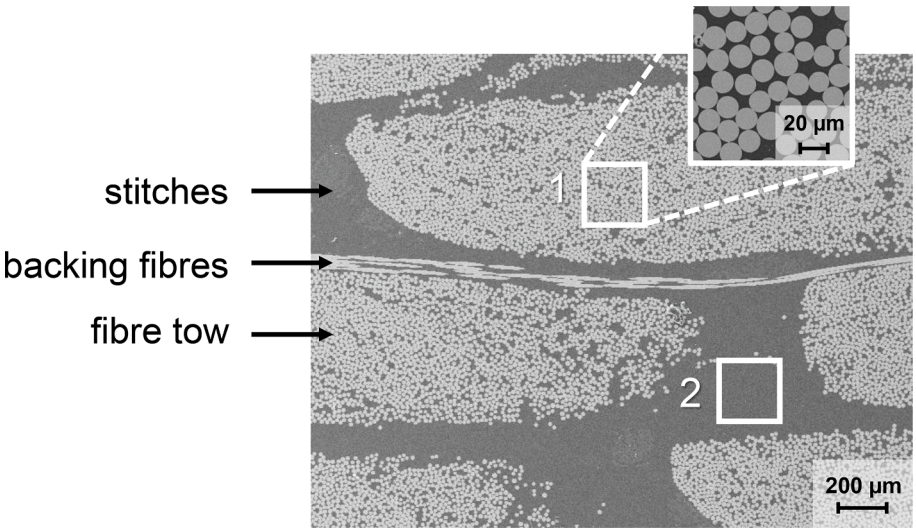

Fig. 1. Scanning electron micrograph of the polished surface of a fibre-reinforced Elium composite specimen after polishing, showing (1) intra-tow and (2) inter-tow matrix pocket morphology.

Table 2
Nomenclature used for describing spatial measurement conditions (i.e. measurement location).

Type of condition	**Spatial (i.e. WHERE measurements were performed)**		
Notation in text/figures	**(1)**	**(2)**	**(3)**
Description	Intra-tow matrix pockets	Inter-tow matrix pockets	Unreinforced resin
Specimen	Composite		Polymer
Distance to nearest fibre	1–20 µm	100–1000 µm	∞ (no fibres in specimen)

300–30 probes (Bruker) were selected as their nominal cantilever spring constant k_c is around 50 N.m^{-1}, i.e. close to the contact stiffness k_N of the tip-Elium resin interaction. Indeed, assuming that (1) E and ν are respectively around 3 GPa and 0.35 for Elium resins, (2) R is usually in the 10–30 nm range for PFT-QNM probes and (3) the maximum value of h must not exceed a few nanometres to ensure the validity of the DMT model (typically $h_{max} \approx 3$ nm), the value of k_N can be estimated at around 40 to 60 N.m^{-1} from eq. (9). Calibration of the photodetector sensitivity, cantilever properties, and PFT-QNM parameters was performed prior to analysis as per the manufacturer's instructions. DMT modulus images of the resin in conditions (1) and (2) (i.e. in the two categories of composite matrix pockets) were acquired at t_0 and t_5 as detailed in Table 3. Note that the fibre–matrix interphase region was also imaged at t_0. In all cases, scan parameters were carefully chosen to ensure that pixel size (i.e. distance between two indented locations) remained larger than contact radius a, so that the probe response was not influenced by adjacent measurement points [64].

The profile extraction tool of the open-source software Gwyddion 2.60 [65] was used to determine the interphase thickness in the composite. Line profiles were manually drawn in several locations across the fibre–matrix interface using 2D property maps obtained in intra-tow areas (condition (1)). Each profile was obtained by averaging the data of 10 neighbouring pixel strips perpendicular to the profile direction in order to reduce noise. Cross-correlation of DMT modulus and PeakForce error data was performed for each profile, and profiles displaying absolute PF error values exceeding 10 % of the applied load were discarded from the study. This kind of artefact reflects an abrupt change in surface topography: it is typically observed in the interface region of composite materials as a result of the differential erosion of the fibre and matrix during polishing. Such a rapid change in surface topography may invalidate the use of the DMT model to determine the modulus if it is the side of the AFM tip that interacts with the surface rather than its apex (in which case the indenter cannot be considered spherical anymore) and/or if the tip slips on the side of the fibre [58]. The thickness of the

Table 3
PFT-QNM AFM acquisition parameters used at t_0 and t_5.

Ageing time of specimens	t_0	t_5
AFM system used	Dimension Icon	MultiMode 8
Probe type	RTESPA-300–30	RTESPA-300
Calibration of cantilever stiffness k_c	49.280 N.m^{-1} (factory calibration)	~ 50 N.m^{-1} (Säder method)
Calibration of tip apex radius R	32 nm (factory calibration)	~ 10 nm (indirect calibration using reference sample, see [64])
Probe vibration frequency	0.5 kHz	2 kHz
PF amplitude	30 nm	20 nm
PF setpoint (i.e. max. applied load P)	150 nN	300 nN
Max. penetration depth h	2–3 nm	
Fit boundaries (for unloading force curve)	Minimum force: 5 % P_{max} Maximum force: 95 % P_{max}	
Scan parameters:		
- Scan size	6 × 6 µm^2 (128 × 128 px^2)	3 × 3 µm^2 (256 × 256 px^2)
- Pixel size	~ 47 nm.px^{-1}	~ 11 nm.px^{-1}
- Scan rate	~ 1 µm.s^{-1}	~ 2 µm.s^{-1}
- Contact radius a	~ 10 nm	~ 9 nm

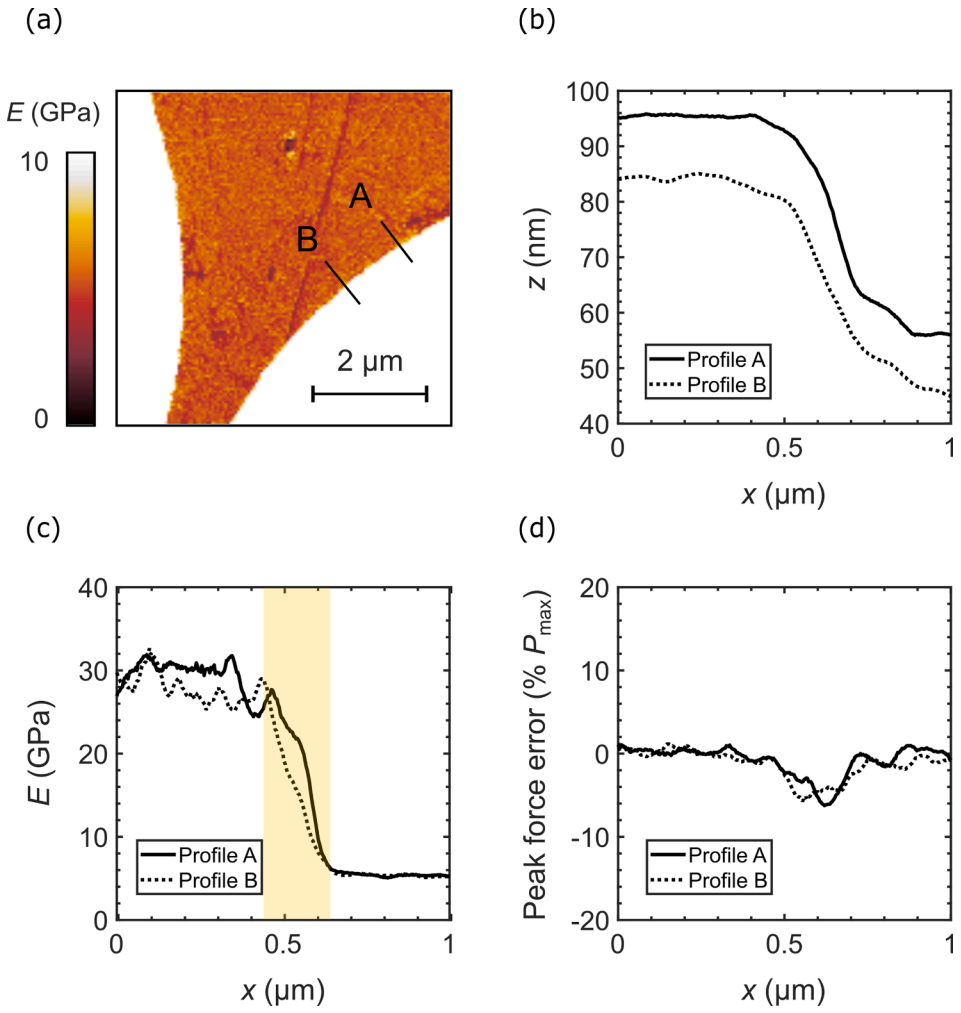

Fig. 2. (a) 2D DMT modulus image obtained by AFM in the intra-tow matrix pocket of the Elium composite with location of 1D profiles A and B, and evolution of (b) topography, (c) DMT modulus and (d) PF error values along profiles A and B.

interphase was measured on the remaining profiles using DMT modulus data. More precisely, the width of the transition zone between the modulus value of the fibre and that of the matrix was assessed graphically as follows. Tangents to each of the three modulus domains (i.e. fibre, interphase, matrix) were drawn on all DMT modulus profiles, resulting in two interception points. The interphase thickness was defined as the difference between the coordinates of the two intercepts.

Intra-tow modulus values beyond the interphase region were then compared to inter-tow (condition (2)) modulus values with Igor Pro 8 (WaveMetrics, Inc., USA), via in-house developed routines. Count histograms were generated from all DMT modulus images with a bin width equal to 50 MPa, excluding outliers (which were defined as modulus values below 1 GPa and above 10 GPa). Results were then accumulated into a single frequency histogram for each measurement condition (i.e. (1) or (2)) and ageing time (i.e. at t_0 or t_5), and fitted with a skew normal probability density function for determining the average modulus and standard deviation values.

3.4. Statistical analysis of nanoindentation results

Nanoindentation datasets were subjected to multiple comparison tests via repeated resampling using R [66] in order to evaluate the influence of the ageing time and distance to nearest fibre on the indentation modulus and hardness of the resin as follows. Let us consider the example of two nanoindentation datasets A and B, consisting of modulus values measured in condition (1) at different ageing times, respectively t_0 and t_3. Each dataset was first resampled down to 60 measurements, which were randomly selected from 8 indents. Resampled datasets A' and B' were compared using a random-intercept linear mixed model expressed as

$$E \sim \underbrace{\text{Ageing time}}_{\text{FIXED EFFECT}} + \underbrace{(1|\text{Indent number}) + (1|\text{Indent batch number})}_{\text{RANDOM EFFECTS}}, \quad (11)$$

where "Ageing time" is the fixed effect, while "Indent number" and "Indent batch number" are random effects. "Indent number" accounts for the fact that each indent yields several modulus measurements in CSM mode. "Indent batch number" is used to illustrate a particulate feature of the nanoindenter operating software, which imposes to perform indents by batches (of about ten indents). Both effects have been found to induce significant variability in the measurements, which is why they have been added to the model as random effects. Possible heteroscedasticity in the compared datasets was also accounted for in the model structure. An estimated difference between datasets A' and B' was obtained from running the model. The resampling/mixed model comparison step was repeated 500 times. The median of the 500 estimated difference values was calculated as well as the 2.5th and 97.5th percentiles, providing a 95 % confidence interval (CI) for the comparison of datasets A and B. In this example, "Ageing time" was the fixed effect while E (indentation modulus of the resin) was the response variable. Depending on the datasets being compared, indentation hardness H can be the variable response instead of E and/or "Fibre proximity" (i.e.

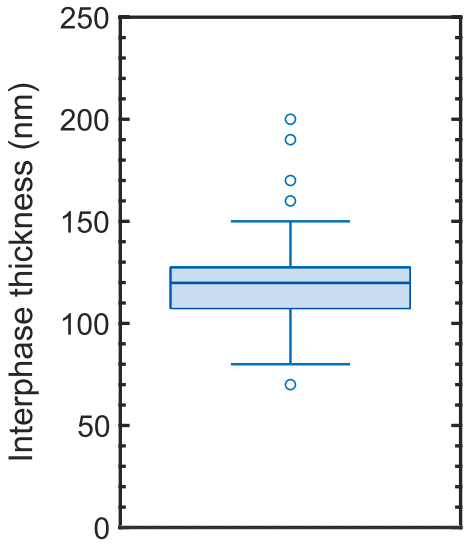

Fig. 3. Box plot distribution of interphase thickness values measured by PFT-QNM AFM in the intra-tow matrix pockets of the Elium composite. Whiskers indicate the minimum and maximum values of the distribution, excluding outliers which are depicted by circles. The box extends between the 25th and 75th percentiles, while the central horizontal line indicates the median value.

condition (1), (2) or (3)) can be the fixed effect instead of "Ageing time'".

4. Results and discussion

4.1. Thickness and mechanical properties of the interphase region

A typical 2D modulus image obtained in an intra-tow matrix pocket of the Elium composite is presented in Fig. 2 alongside the evolution of the topography, DMT modulus and PF error values along two 1 μm long 1D profiles drawn across the fibre–matrix interface. The modulus profiles in Fig. 2c exhibit an upper plateau around 30 GPa and a lower plateau close to 5.5 GPa, which are attributed to the fibre and matrix materials, respectively. Modulus measurements appear more scattered in the glass fibre than in the polymer, and also have significantly lower values than the macroscopic modulus of glass (~ 70 GPa). As explained previously, the cantilever stiffness of the AFM probe was selected to be close to the contact stiffness between the tip and the polymer. Hence, the probe is too compliant to properly indent the fibre surface, which results in unrealistic modulus measurements in this material and low signal-to-noise ratio as the lower the indentation depth, the larger the impact of surface roughness on modulus measurements [8,17]. Consistently with the finding already reported in [23], a ~ 150 nm transition zone in which the DMT modulus decreases almost linearly from 30 to 5.5 GPa is observed between the fibre and matrix phases, as depicted by the yellow area in Fig. 2c.

The AFM indentation of the Elium polymer close to a fibre was also modelled via FE simulation, in order to decouple fibre constraint effects from an actual change in polymer properties close to the fibre–matrix interface. The results of these simulations, which are presented in the Supplementary Information, confirm that this behaviour does not result from a constraining effect from the fibre material. The 150-nanometre-thick strip of material surrounding the fibre in Fig. 2 is thus intrinsically different from the polymer found further away from the fibre–matrix interface and, as such, constitutes a phase of its own (with respect to the two other phases, i.e. the fibre and matrix). This "third phase", which appears stiffer than the composite matrix and exhibits a property gradient across the thickness is likely to be the interphase region. Note that a change in topography occurs as a consequence of the differential erosion of the fibre and matrix materials during polishing, giving rise to an inclined surface characterised by the "slope angle" Φ. The presence of an inclined surface in the interphase region should not impact the accuracy of the modulus measurements, provided the following conditions are met. First, the probe tip must remain in contact with the surface at all times, which is confirmed by the low PF error values displayed in Fig. 2d. The PF error does not exceed 6 % of the applied load in the interphase region, which would approximately translate into a 6 % error in the calculated DMT modulus value, see eq. (9). Second, the value of the slope angle Φ should be accounted for in the determination of E^* from eq. (9) as follows [67]:

$$E^*_{\phi\neq 0} = \left(\frac{dP}{dh}\right)\frac{1}{2h\sqrt{R}}\frac{1}{\sqrt[3]{\cos\phi}} \tag{12}$$

In practice, the influence of Φ on the calculated value of E^* can be considered negligible as long as the value of Φ remains small. In this work, only interphase regions for which the $\Phi < 0.1$ rad criterion was met (which is equivalent to a maximum 10 % slope) were characterised by AFM, as exemplified in Fig. 2b. Therefore, from eq. (12), the error on

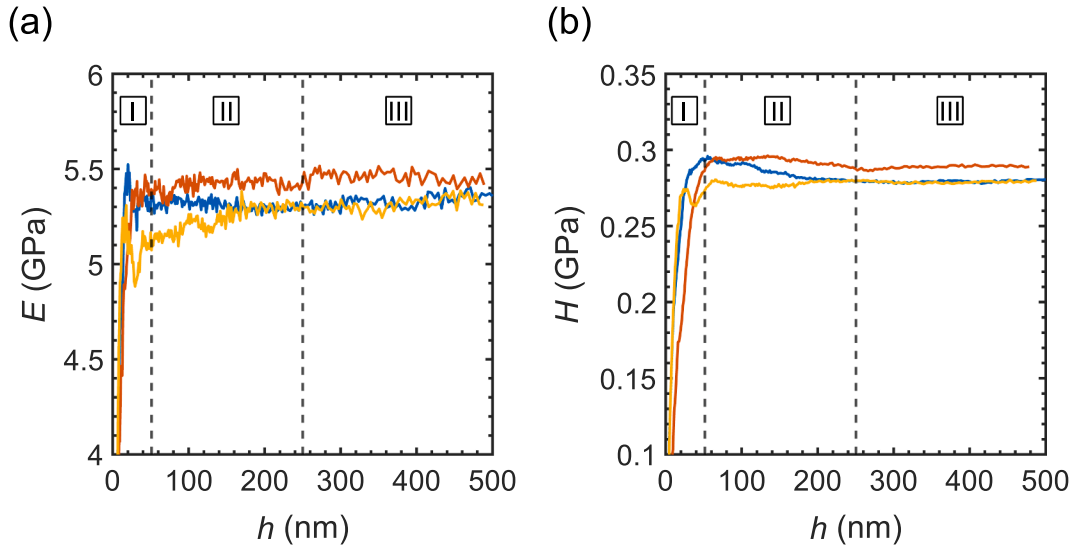

Fig. 4. Typical evolution of (a) E and (b) H values measured by nanoindentation in Elium as a function of the penetration depth h. Each colour represents one indent performed in the bulk polymer (i.e. condition (3)) at t_5.

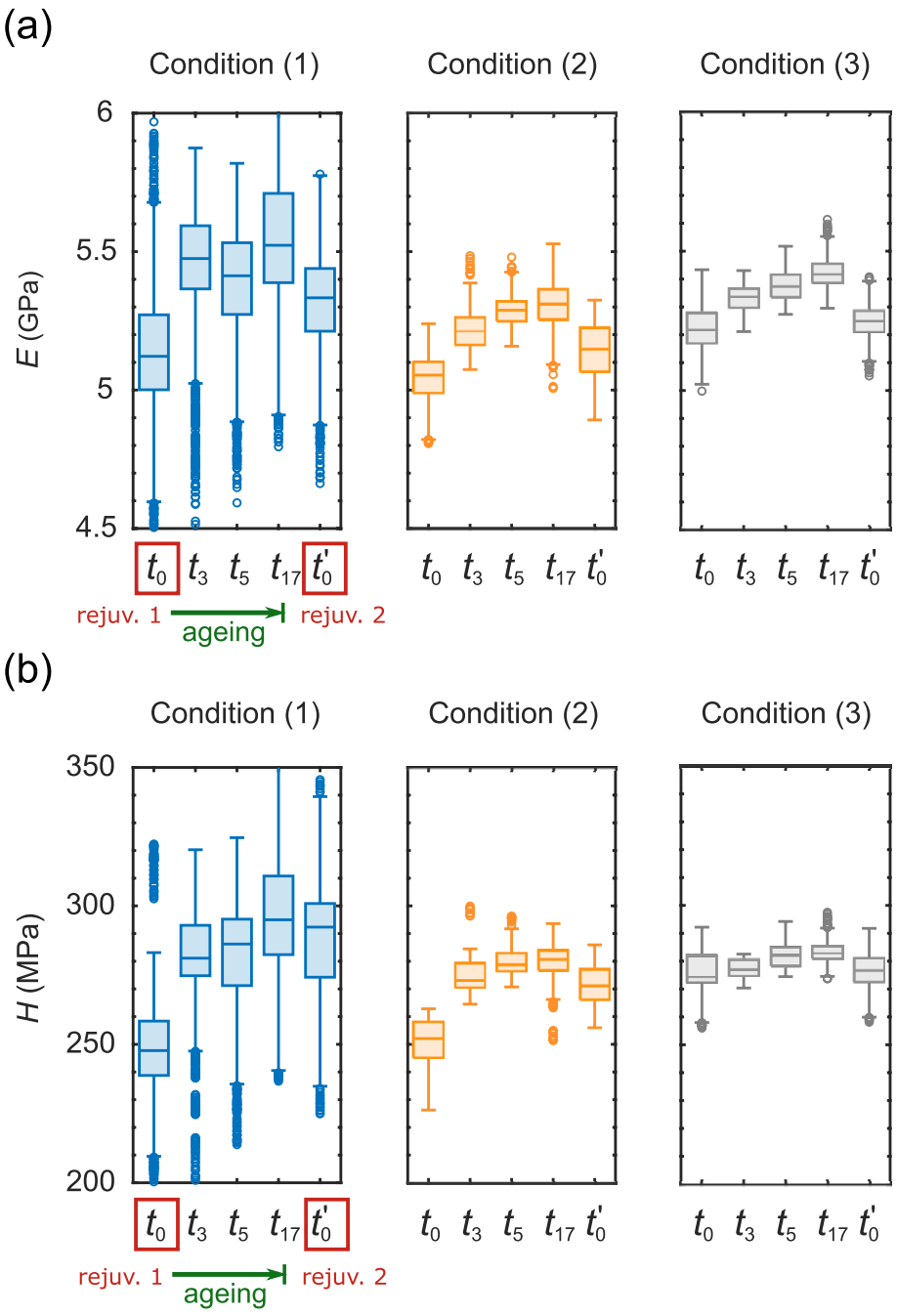

Fig. 5. Box plot distributions of (a) E and (b) H values measured by nanoindentation in conditions (1), (2) and (3), for several values of the ageing time. Whiskers indicate the minimum and maximum values of each distribution, excluding outliers which are depicted by circles. Boxes extend between the 25th and 75th percentiles, while the central horizontal line indicates the median value.

the calculated value of E^* resulting from differential erosion should not exceed ~ 0.2 %.

The distribution of interphase thickness values measured by PFT-QNM AFM is shown in Fig. 3. The box plot is symmetric, which suggests a normal distribution of interphase thickness values (provided the data is unimodal, which is the case here). The median and mean values are both approximately equal to 120 nm, while the calculated standard deviation is around 30 nm. The maximum measured thickness value, including outliers, does not exceed 200 nm. The radius of the glass fibres used as reinforcement in the composite material is approximately 7.5 μm, and the smallest possible matrix pocket could be defined as the closed space between 3 mutually tangent fibres. The cross-sectional area of this "smallest pocket" can be estimated through simple geometric calculations; it is around 9 μm^2. Considering the extreme case of a 200-nm interphase region extending from the surfaces of the three tangent fibres, less than half of the total area of the "smallest pocket" would be occupied by the interphase. This ratio decreases to around ¼ if we assume an interphase thickness value of 120 nm. This confirms that even the smallest intra-tow matrix pockets are mostly composed of the Elium polymer, not of a continuous interphase region.

4.2. Influence of fibre proximity and physical ageing on nanoindentation response

4.2.1. Selection of nanoindentation data for statistical analysis

Indents performed in CSM mode yield one data point for each 1 nm

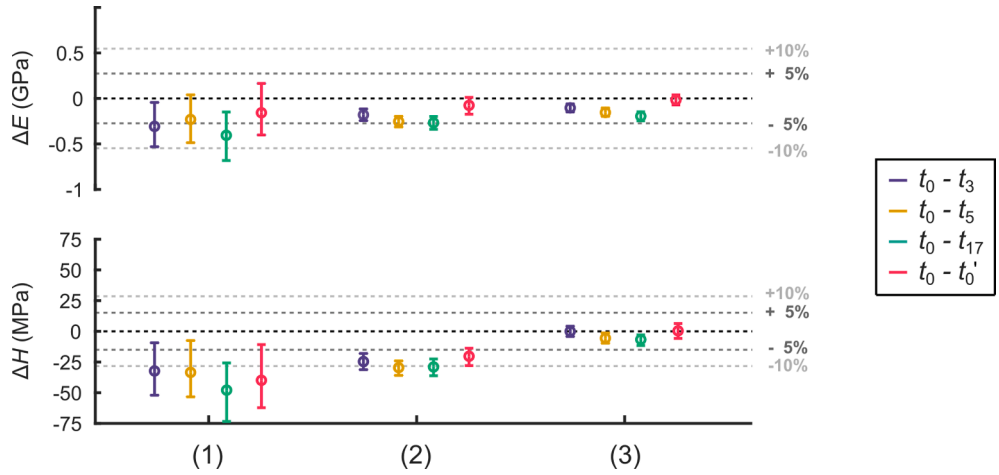

Fig. 6. Median differences (circles) and 95 % CIs (error bars) in (a) *E* and (b) *H* values, obtained from the pairwise comparison of nanoindentation datasets acquired at different aging times for the same measurement condition (i.e. (1), (2) or (3)). The grey dotted lines indicate variations of ± 5 or 10 % with respect to the average values of *E*, i.e. 5.3 GPa and *H*, i.e. 280 MPa.

variation of the penetration depth *h*. This results in a considerable amount of data, which are not all relevant with respect to the present study. In particular, the CSM nanoindentation curves systematically exhibit important fluctuations at low penetration depths for a variety of reasons (see e.g. [26,68–71]). In the case of interest, the measured values of *E* and *H* decrease as *h* decreases towards 0. The typical evolution of *E* and *H* as a function of *h* is shown in Fig. 4 for three random indents performed in the bulk Elium specimen. The *E* and *H* plots are divided into three domains with respect to the penetration depth *h*, see Fig. 4a and 4b, respectively. In domain I, i.e. for $0 < h \lesssim 50$ nm, *E* and *H* values exhibit very sharp fluctuations. Slighter variations are observed in domain II, which extends from $h \sim 50$ to $h \sim 250$ nm. In domain III, i.e. for $h > 250$ nm, all *E* and *H* curves reach a plateau, meaning that the measurements are no longer dependent on the penetration depth. Note that the behaviour illustrated by Fig. 4 was observed regardless of fibre proximity (i.e. condition (1), (2) or (3)) and ageing time, in both *E* and *H* data. A similar evolution for $h < 100$ nm has already been observed when indenting poly(methyl methacrylate) [71], which is the main constituent of Elium after polymerisation. The phenomenon was attributed to uncertainties in the measured displacements as well as in the contact determination due to tip blunting [71].

In light of these observations, only *E* and *H* measurements acquired in the range $400 < h < 450$ nm (i.e. in domain III) were included in the statistical analysis for conditions (2) and (3). For condition (1), however, narrowing down the datasets obtained from each indent was not as straightforward. As mentioned in the introduction, the indentation response of composite matrix pockets may be affected by the proximity of the stiffer reinforcing material. FE models of nanoindentation experiments [24–26,37] are classically used to quantify this "constraining effect" as a function of the *x/h* ratio, where *x* is the distance between the indenter tip and the closest fibre–matrix interface and *h* is the penetration depth. A critical *x/h* value is identified from the FE simulations, above which the indentation measurements should no longer be impacted by the fibre response. A similar FE study was performed for the Elium composite, as described in the Supplementary Information. The simulation results showed that *E* and *H* measurements could be considered unconstrained for $x/h > 30$. However, as *x/h* increases above this critical value, the measurements may become affected instead by the variability observed previously at low indentation depths - whatever its origin may be [24,26]. Finding the "sweet spot", i.e. a range of *x/h* values to avoid both the constraining effect and the low-depth experimental variability, is challenging – if not impossible. As FE simulations like those performed in this work do not capture the variability at low depths, an upper bound for the *x/h* ratio can only be estimated from the

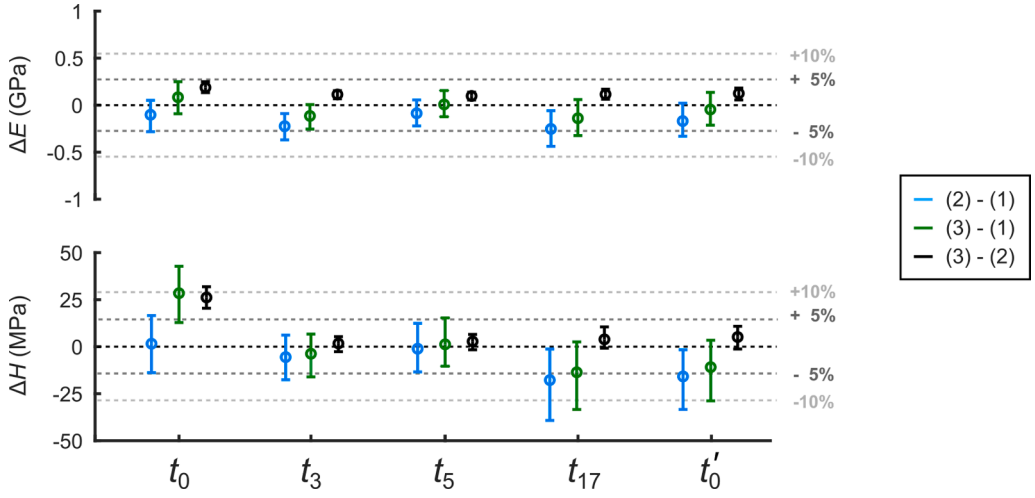

Fig. 7. Median differences (circles) and 95 % CIs (error bars) in (a) *E* and (b) *H* values, obtained from the pairwise comparison of nanoindentation datasets acquired in conditions (1), (2) and (3) at the same ageing time. The grey dotted lines indicate variations of ± 5 or 10 % with respect to the average values of *E*, i.e. 5.3 GPa and *H*, i.e. 280 MPa.

experimental results. In this work, the maximum acceptable value of x/h was set to 40 for the following reason. From image analysis, the minimum radius x of the analysed intra-tow matrix pockets is known to be around 2 μm. The variability at low depths is most significant in domain I, i.e. for h values below 50 nm, according to the previous paragraph. Hence, any data point meeting the condition $30 < x/h < 40$ (=2,000/50) should not be affected by fibre constraint nor be too impacted by the variability at low depth. In practice, nearly all data points obtained for condition (1) belong to domain II. This is due to the fact that $x < 10$ μm for 95 % of the analysed matrix pockets, resulting in unconstrained responses for penetration depths below 300 nm.

4.2.2. *Descriptive and inference statistical analysis of nanoindentation results*

The distributions of E and H values obtained by nanoindentation in conditions (1), (2) and (3) at different ageing times are presented in Fig. 5. All box plots appear relatively symmetric, suggesting that each dataset follows a close-to-normal distribution (again, provided the data is unimodal, which has been verified in all cases). In each plot, box height represents the interquartile range, which allows estimating the variability of a dataset. Box height is, on average, twice larger for E and H datasets corresponding to condition (1) compared to conditions (2) and (3), indicating a wider dispersion of nanoindentation measurements performed in intra-tow matrix pockets. This results from the fact that most unconstrained data points obtained for condition (1) are slightly impacted by the variability at low depths, as mentioned in the previous section.

Despite this difference in variability, the data shown in Fig. 5 provide insight into the influence of fibre proximity and physical ageing on the nanoindentation response of the resin. The majority of E and H values in Fig. 5a and 5b lie within the 5.3 ± 10 % GPa and 280 ± 10 % MPa ranges, respectively. Regardless of fibre proximity, a clear trend emerges with respect to the effect of the ageing time on the mechanical properties of the resin. More precisely, E and H values increase with the "physical age" of the resin, and drop following the second thermal rejuvenation treatment (which corresponds to t_0'). The largest increase in E and H values occurs during the first 3 months following the initial rejuvenation treatment, i.e. between t_0 and t_3. There seems to be, however, an influence of fibre proximity on the extent of the observed variations. The largest apparent increase in properties with physical age is respectively observed in condition (1), then (2) and eventually (3). In particular, the median value of H increases by ~ 20 % between t_0 and t_{17} for condition (1), by ~ 10 % for condition (2) and by less than 5 % for condition (3), see Fig. 5b. A similar tendency is observed for E values shown in Fig. 5a, though to a lesser extent. This indicates a higher "physical ageing potential" for the resin located in the close vicinity of fibres, which is consistent with the conclusions drawn by Cangialosi and co-workers [46–48] in the case of PMMA reinforced with silica nanoparticles. Surprisingly, however, the second rejuvenation treatment induces the same 3 % drop in the median value of E and H between t_{17} and t_0' for all conditions, except in one case (the decrease in the median H value for condition (1) seems more subtle - likely between 0 and 1 %). As a consequence, condition (3) is the only one exhibiting the same nanoindentation response at t_0 and t_0', i.e. after the first and second rejuvenation treatments. The resin properties in condition (2) and especially (1) remain larger at t_0' than at t_0.

The results presented in Fig. 5 yield interesting conclusions, which can be further analysed via inference statistics. Figs. 6 and 7 present the 95 % CIs obtained from multiple pairwise comparisons performed between nanoindentation datasets for assessing the respective influence of fibre proximity (i.e. condition (1), (2) or (3)) and ageing time on the mechanical properties of the resin. CIs should be interpreted as follows: if the interval contains 0, the corresponding difference is deemed non-significant from a statistical point of view. If a CI does not contain 0, there is a 95 % probability that the two datasets being compared are different: the result is statistically significant. Yet, a statistically significant difference is not always considered "important", depending on the overall purpose of the study. Here, grey dotted lines in Figs. 6 and 7 indicate a ± 5 % or ± 10 % difference with respect to the aforementioned baseline values of 5.3 GPa for E and 280 MPa for H. In this work, any statistically significant difference whose CI lies completely outside the ± 5 % range is considered important from a mechanical viewpoint.

The variations in the modulus and hardness of the resin in conditions (1), (2) and (3) as ageing time increases are respectively depicted in the top and bottom parts of Fig. 6. Inter-tow matrix pockets (condition (2)) do not experience important variations in modulus values due to physical ageing, while hardness values increase by more than 5 % between t_0 and t_3, nearly exceeding the 10 % difference threshold by t_{17}. The comparisons made on pure resin (condition (3)), on the other hand, suggest no important changes in neither the modulus nor hardness values with increasing ageing time. The larger dispersion of measurements previously observed in intra-tow matrix pockets translates into larger confidence intervals for condition (1). While this impacts the statistical significance of most of the corresponding CIs, the comparison of nanoindentation datasets obtained at t_0 and t_{17} still clearly shows an increase in hardness values of at least 10 % in intra-tow matrix pockets.

We note in passing that the hardness comparisons performed between t_0 and t_0' for the three conditions confirm the observations made from Fig. 5, i.e. intra- and inter-tow matrix pockets do not recover their "initial" (t_0) properties after the second thermal rejuvenation treatment. The possible explanations for this are the following. First, despite the precautions taken to ensure a complete relaxation of the polymer, the second treatment may not have been carried out at a sufficiently high temperature and/or for long enough to completely reverse the effects of physical ageing in the composite matrix. Otherwise, part of the increase in hardness values over time may result from another chemical or physical phenomenon which has not been yet formally identified. The belated polymerisation of some residual monomer and/or the progressive loss of some volatile compounds present in the Elium polymer is another potential explanation, as suggested by the DSC measurements shown in the Supplementary Information. However, this assumption remains to be confirmed, as the increase in properties between t_0 and t_0' is only observed for conditions (1) and (2), while condition (3) achieves a full recovery of the initial properties after the second thermal rejuvenation.

The effect of fibre proximity on the nanoindentation response of the resin is shown in Fig. 7 for several levels of physical ageing. There is no important effect of fibre proximity on the resin modulus, whatever the ageing time considered. Differences in resin hardness, which are depicted in the bottom part of Fig. 7, yield essentially the same conclusions. Still, at t_0, the pure resin (condition (3)) exhibits more than 5 % higher hardness values than the inter-tow composite matrix pockets (condition (2)), and probably also than the intra-tow matrix pockets (condition (1)) although the CI slightly intercepts the + 5 % line. This initial mismatch could result from small differences in residual monomer content between the composite and bulk resin specimens and/or from the additional presence of the glass fibre sizing in the case of the composite - both residual methyl methacrylate and glass fibre sizing components having a strong plasticising effect on PMMA-based Elium resins, even at very low concentrations [62]. More interesting is the fact that the difference in hardness between the pure resin and the composite matrix is no longer observed as ageing time increases. We know from Fig. 6 that the composite matrix (i.e. conditions (1) and (2)) is more affected by physical ageing than pure resin (condition (3)). As physical ageing manifests itself by an increase of the hardness and modulus values, the difference in hardness between the bulk resin and the composite matrix at t_0 is thus "smoothed out" as the ageing time increases.

Two partial conclusions can be drawn from the results presented in this section. First, whatever the ageing time considered, the measured differences between bulk and local Elium properties remain smaller than those reported by Gregory and Spearing [24], Hardiman [25], Chevalier [37] and Pecora [29] for various epoxy systems - which should be taken

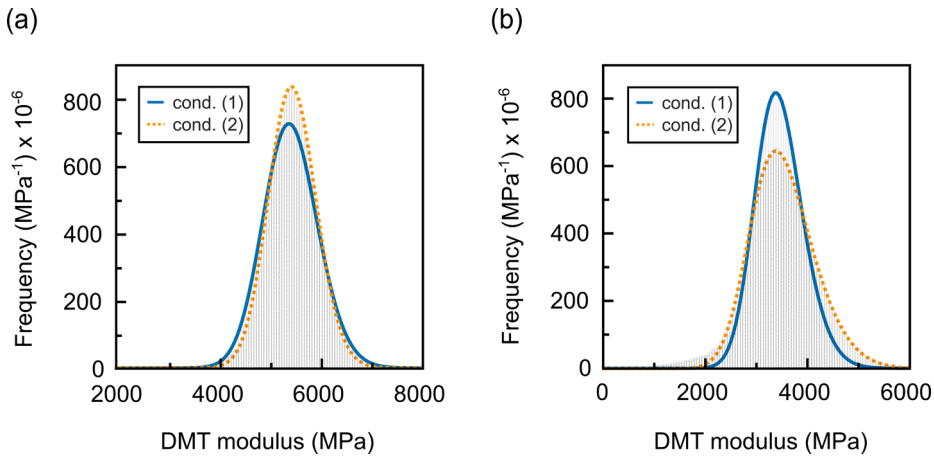

Fig. 8. Histogram distribution and skew gaussian fit of DMT modulus values measured by AFM in intra-tow (condition (1)) versus inter-tow (condition (2)) composite matrix pockets at (a) t_0 and (b) t_5.

as an advantage. Indeed, the resins developed for liquid composite moulding processes are first characterised and optimised in bulk form, whose properties (e.g. in terms of mechanical response) are expected to be transposable to the corresponding fibre-reinforced polymer system. Secondly, the slight change in the composite matrix properties related to ageing seem to mostly occur within the first three months after rejuvenation. Therefore, imposing a three-month waiting time between the manufacturing and the mechanical testing of Elium composite parts could further enhance the representativeness of the characterisation results, at least for the particular fibre–matrix system studied in this work.

4.3. Comparison with PFT-QNM AFM measurements

Histograms showing the distributions of DMT modulus values obtained by AFM in intra-tow (condition (1)) versus inter-tow (condition (2)) matrix pockets at t_0 and t_5 are presented in Fig. 8 alongside their fitted skew-normal probability density functions. As explained in section 2.1, the modulus values obtained by AFM in this work are considered relative, i.e. only comparable with data obtained in the same experimental conditions (same probe, same calibration and operating parameters). Consequently, the data obtained at t_0 (see Fig. 8a) and t_5 (see Fig. 8b) cannot be compared in a quantitative manner, as they correspond to two different sets of experimental conditions (in terms of AFM device, probe type and calibration parameters, see section 3.3). From the equations of the fitted probability density functions shown in Fig. 8a, the mean value and standard deviation of the DMT modulus distributions at t_0 can be estimated. These are respectively equal to 5,036 $\pm$ 660 MPa for condition (1) and 5,164 $\pm$ 550 MPa for condition (2). Following the same approach for Fig. 8b, the calculated values of the mean modulus and standard deviation at t_5 are equal to 3,930 $\pm$ 600 MPa for condition (1) and to 3,950 $\pm$ 720 MPa for condition (2). These results reinforce one of the conclusions drawn from the nanoindentation measurements with respect to the absence of significant differences in modulus values between conditions (1) and (2) at t_0 and t_5. We note in passing that the dispersion of AFM measurements is in the same order of magnitude for both conditions: AFM is especially designed for providing accurate measurements at very low (or even zero) indentation depths, contrary to nanoindentation measurements whose accuracy at penetration depths below 100 nm is limited, as mentioned above.

5. Conclusions

The effects of physical ageing and fibre proximity on the local mechanical response of a methacrylic resin were assessed by CSM nanoindentation and PFT-QNM AFM indentation. The main findings of the present study are the following. The modulus and hardness of the resin do not significantly vary as a function of fibre proximity (excluding the 100- to 200-nanometre-thick interphase region), provided all tested specimens have been subjected to the same level of natural physical ageing up to 17 months. Second, there is a slight influence of fibre proximity on the rate and extent of physical ageing experienced by the resin, i.e. intra-tow matrix pockets show earlier and stronger signs of ageing (in particular via an increase of the hardness) than inter-tow matrix pockets and unreinforced resin, respectively. Third, most of the increase in indentation properties related to physical ageing is already achieved three months after the rejuvenation treatment, whatever the level of fibre proximity. Therefore, imposing a three-month waiting period between the processing and mechanical characterisation of an Elium 191O/SA composite part will improve the representativeness of the test results. Last, while the properties of the composite matrix remain comparable to those of the bulk polymer within the timescale of the study, i.e. for at least 17 months, the observed difference in ageing behaviour could, in the longer run, lead the composite matrix properties to diverge significantly from those of the bulk polymer, as observed by several authors in the case of epoxy resin systems. Further work could therefore focus on the following questions:

- What is the effect of longer periods of natural ageing time (>18 months) on the mechanical response of unreinforced and reinforced Elium resins? Do their properties stop evolving after a certain amount of time? If they do, this could help determine the best timing for performing the mechanical characterisation of a composite part after it has been manufactured.

- Can the results of accelerated ageing studies (performed at temperatures higher than room temperature) be reliably extrapolated to predict the long-term behaviour of polymers and polymer composites exposed to natural ageing conditions? This matter is still debated in the literature, see e.g. [72].

CRediT authorship contribution statement

Sarah F. Gayot: Conceptualization, Data curation, Formal analysis, Investigation, Methodology, Software, Visualization, Writing – original draft, Writing – review & editing. **Nathan Klavzer:** Data curation, Software. **Alain Guillet:** Formal analysis, Methodology, Software. **Christian Bailly:** Supervision, Writing – review & editing. **Pierre Gérard:** Resources, Supervision. **Thomas Pardoen:** Supervision, Writing – review & editing. **Bernard Nysten:** Formal analysis, Investigation, Software, Supervision, Writing – review & editing.

Declaration of competing interest

The authors declare that they have no known competing financial interests or personal relationships that could have appeared to influence the work reported in this paper.

Data availability

Data will be made available on request.

Acknowledgments

Financial support from Arkema and the Fonds de la Recherche Scientifique de Belgique (FNRS) is gratefully acknowledged. The authors would like to thank the Elium team at Arkema Lacq (France) for their assistance with composite manufacturing, as well as the following people for providing their help and guidance: Dr Audrey Favache and Ms Sophie Ryelandt with nanoindentation, Ms Cécile D'Haese and Pr Philippe Leclère with AFM and Ms Catherine Rasse with statistical analyses.

Appendix A. Supplementary material

Supplementary data to this article can be found online at https://doi.org/10.1016/j.compositesa.2024.108141.

References

[1] LLorca J, González C, Molina-Aldareguía JM, Segurado J, Seltzer R, Sket F, et al. Multiscale modeling of composite materials: A roadmap towards virtual testing. Adv Mater 2011;23:5130–47.
[2] LLorca J, González C, Molina-Aldareguía JM, Lópes CS. Multiscale modeling of composites: Toward virtual testing and beyond. JOM 2013;65:215–25.
[3] Kim J-K, Mai Y-W. Engineered Interfaces in Fiber Reinforced Composites. 1st edition. Elsevier Science; 1998.
[4] Vanlandingham MR, McKnight SH, Palmese GR, Bogetti TA, Eduljee RF, Gillespie JW. Characterization of interphase regions using atomic force microscopy. MRS Proc 1996;458:313. https://doi.org/10.1557/PROC-458-313.
[5] VanLandingham MR, Villarrubia JS, Meyers G. Nanoindentation of polymers: Tip shape calibration and uncertainty. Issues 1999;41(2):1412–3.
[6] Downing TD, Kumar R, Cross WM, Kjerengtroen L, Kellar JJ. Determining the interphase thickness and properties in polymer matrix composites using phase imaging atomic force microscopy and nanoindentation. J Adhes Sci Technol 2000;14:1801–12.
[7] Syed Asif SA, Wahl KJ, Colton RJ, Warren OL. Quantitative imaging of nanoscale mechanical properties using hybrid nanoindentation and force modulation. J Appl Phys 2001;90:1192–200.
[8] Gao S-L, Mader E. Characterisation of interphase nanoscale property variations in glass fibre reinforced polypropylene and epoxy resin composites. Compos Part A Appl Sci Manuf 2002;33:559–76.
[9] He JM, Huang YD. AFM characterization of interphase properties of silver-coated carbon fibre reinforced epoxy composites. Polym Polym Compos 2006;14:123–34. https://doi.org/10.1177/096739110601400201.
[10] Wang Y, Hahn TH. AFM characterization of the interfacial properties of carbon fiber reinforced polymer composites subjected to hygrothermal treatments. Compos Sci Technol 2007;67:92–101.
[11] Wang SQ, Nair SD, Hurley D, Lee SH. Characterizing interphase properties in fiber reinforced polymer composite with advanced AFM based tools. Adv Mat Res 2010;123–125:403–6.
[12] Qu M, Deng F, Kalkhoran SM, Gouldstone A, Robisson A, Van Vliet KJ. Nanoscale visualization and multiscale mechanical implications of bound rubber interphases in rubber–carbon black nanocomposites. Soft Matter 2011;7:1066–77.
[13] Cech V, Palesch E, Lukes J. The glass fiber–polymer matrix interface/interphase characterized by nanoscale imaging techniques. Compos Sci Technol 2013;83:22–6.
[14] Cheng X, Putz KW, Wood CD, Brinson LC. Characterization of local elastic modulus in confined polymer films via AFM indentation. Macromol Rapid Commun 2015;36:391–7.
[15] Brune PF, Blackman GS, Diehl T, Meth JS, Brill D, Tao Y, et al. Direct measurement of rubber interphase stiffness. Macromolecules 2016;49:4909–22. https://doi.org/10.1021/acs.macromol.6b00689.
[16] Zhang M, Li Y, Kolluru PV, Brinson LC. Determination of mechanical properties of polymer interphase using combined atomic force microscope (AFM) experiments and finite element simulations. Macromolecules 2018;51:8229–40.
[17] Babu LK. The use of AFM indentation to quantify mechanical properties of the interphase region in fiber-reinforced composites. Oklahoma State University; 2019.
[18] Hodzic A, Stachurski ZH, Kim JK. Nano-indentation of polymer–glass interfaces Part I. Experimental and mechanical analysis. Polymer 2000;41:6895–905. https://doi.org/10.1016/S0032-3861(99)00890-3.
[19] Kim J-K, Sham M-L, Wu J. Nanoscale characterisation of interphase in silane treated glass fibre composites. Compos Part A Appl Sci Manuf 2001;32:12.
[20] Wu Q, Li M, Gu Y, Li Y, Zhang Z. Nano-analysis on the structure and chemical composition of the interphase region in carbon fiber composite. Compos Part A Appl Sci Manuf 2014;56:143–9. https://doi.org/10.1016/j.compositesa.2013.10.003.
[21] Wu Q, Li M, Gu Y, Wang S, Zhang Z. Imaging the interphase of carbon fiber composites using transmission electron microscopy: Preparations by focused ion beam, ion beam etching, and ultramicrotomy. Chin J Aeronaut 2015;28:1529–38. https://doi.org/10.1016/j.cja.2015.05.005.
[22] Gu Y, Li M, Wang J, Zhang Z. Characterization of the interphase in carbon fiber/polymer composites using a nanoscale dynamic mechanical imaging technique. Carbon 2010;48:3229–35. https://doi.org/10.1016/j.carbon.2010.05.008.
[23] Klavzer N, Gayot SF, Coulombier M, Nysten B, Pardoen T. Nanoscale digital image correlation at elementary fibre/matrix level in polymer–based composites. Compos Part A Appl Sci Manuf 2023;168:107455. https://doi.org/10.1016/j.compositesa.2023.107455.
[24] Gregory J, Spearing S. Nanoindentation of neat and polymers in polymer-matrix composites. Compos Sci Technol 2005;65:595–607.
[25] Hardiman M, Vaughan TJ, McCarthy CT. The effect of fibre constraint in the nanoindentation of fibrous composite microstructures: A finite element investigation. Comput Mater Sci 2012;64:162–7.
[26] Hardiman M, Vaughan TJ, McCarthy CT. Fibrous composite matrix characterisation using nanoindentation: The effect of fibre constraint and the evolution from bulk to in-situ matrix properties. Compos Part A Appl Sci Manuf 2015;68:296–303.
[27] Hardiman M, Vaughan T, McCarthy C. The effect of microscale residual stress from thermal cooldown on the nanoindentation properties of fibre-reinforced composites. J Compos Mater 2016;50:4147–58. https://doi.org/10.1177/0021998316632603.
[28] Hardiman M, Vaughan TJ, McCarthy CT. The effects of pile-up, viscoelasticity and hydrostatic stress on polymer matrix nanoindentation. Polym Test 2016;52:157–66.
[29] Pecora M, Smerdova O, Gigliotti M. In-situ characterization of the local mechanical behaviour of polymer matrix in 3D carbon fiber composites by cyclic indentation test. Compos Struct 2020;244:112268. https://doi.org/10.1016/j.compstruct.2020.112268.
[30] Pardoen T, Klavzer N, Gayot S, Van Loock F, Chevalier J, Morelle X, et al. Nanomechanics serving polymer-based composite research. C R Phys 2021;22:331–52. https://doi.org/10.5802/crphys.56.
[31] Gates T. The physical and chemical ageing of polymeric composites. Ageing of composites. 1st edition. Woodhead Publishing; 2008.
[32] Yedla SB, Kalukanimuttam M, Winter RM, Khanna SK. Effect of shape of the tip in determining interphase properties in fiber reinforced plastic composites using nanoindentation. J Eng Mater Technol 2008;130:1–15. https://doi.org/10.1115/1.2975234.
[33] Díez-Pascual AM, Gómez-Fatou MA, Ania F, Flores A. Nanoindentation assessment of the interphase in carbon nanotube-based hierarchical composites. J Phys Chem C 2012;116:24193–200. https://doi.org/10.1021/jp309067e.
[34] Li Y, Li M, Gu Y, Zhang Z, Guan P. Investigation of the nanoscale mechanical properties of carbon fiber/epoxy resin interphase. I. analysis of fiber-stiffening effect during the nanoindentation process based on numerical simulation. Polym Compos 2012;33:1387–94. https://doi.org/10.1002/pc.22265.
[35] Hu Z, Lynne KJ, Markondapatnaikuni SP, Delfanian F. Material elastic–plastic property characterization by nanoindentation testing coupled with computer modeling. Mater Sci Eng A 2013;587:268–82. https://doi.org/10.1016/j.msea.2013.08.071.
[36] Hu Z, Farahikia M, Delfanian F. Fiber bias effect on characterization of carbon fiber-reinforced polymer composites by nanoindentation testing and modeling. J Compos Mater 2015;49:3359–72.
[37] Chevalier J. Micromechanics of an epoxy matrix for fiber reinforced composites : experiments and physics-based modelling. Université catholique de Louvain, 2018.
[38] Struik LCE. Physical aging in amorphous polymers and other materials. Technische Hogeschool Delft, 1977.
[39] Flory A, McKenna GB. Physical aging behavior of the normal force and torque in polymer glasses. Mech Time-Depend Mater 2010;14:347–57. https://doi.org/10.1007/s11043-010-9114-9.
[40] Hastie RL, Morris DH. The effect of physical aging on the creep response of an off-axis thermoplastic composite. vol. 1, Las Vegas, NV: 1992, p. 183–91.
[41] Sullivan JL, Blais EJ, Houston D. Physical aging in the creep behavior of thermosetting and thermoplastic composites. Compos Sci Technol 1993;47:389–403. https://doi.org/10.1016/0266-3538(93)90008-5.
[42] McKenna GB. On the physics required for prediction of long term performance of polymers and their composites. J Res Natl Inst Stan J 1994;99:169. https://doi.org/10.6028/jres.099.014.
[43] Leveque D, Schieffer A, Mavel A, Maire J. Analysis of how thermal aging affects the long-term mechanical behavior and strength of polymer?matrix composites. Compos Sci Technol 2005;65:395–401. https://doi.org/10.1016/j.compscitech.2004.09.016.
[44] Martin R. Ageing of Composites. 1st edition. Woodhead Publishing In Materials; 2008.
[45] Odegard GM, Bandyopadhyay A. Physical aging of epoxy polymers and their composites. J Polym Sci B Polym Phys 2011;49:1695–716. https://doi.org/10.1002/polb.22384.

[46] Boucher VM, Cangialosi D, Alegría A, Colmenero J, González-Irun J, Liz-Marzan LM. Accelerated physical aging in PMMA/silica nanocomposites. Soft Matter 2010;6:3306. https://doi.org/10.1039/c001656j.
[47] Cangialosi D, Boucher V, Alegría A, Colmenero J. Free volume holes diffusion to describe physical aging in poly(mehtyl methacrylate)/silica nanocomposites. J Chem Phys 2011;135:014901. https://doi.org/10.1063/1.3605600.
[48] Cangialosi D, Boucher VM, Alegría A, Colmenero J. Physical aging in polymers and polymer nanocomposites: recent results and open questions. Soft Matter 2013;9:8619. https://doi.org/10.1039/c3sm51077h.
[49] Fischer-Cripps AC. Nanoindentation. New York, NY: Springer New York; 2011. https://doi.org/10.1007/978-1-4419-9872-9.
[50] Oliver WC, Pharr GM. An improved technique for determining hardness and elastic modulus using load and displacement sensing indentation experiments. J Mater Res 1992;7:1564–83.
[51] Pittenger B, Erina N, Su C. Quantitative Mechanical Property Mapping at the Nanoscale with PeakForce QNM n.d.
[52] Derjaguin BV, Muller VM, Toporov YP. Effect of contact deformations on the adhesion of particles. J Colloid Interface Sci 1975;53:314–26. https://doi.org/10.1016/0021-9797(75)90018-1.
[53] Clifford CA, Seah MP. Quantification issues in the identification of nanoscale regions of homopolymers using modulus measurement via AFM nanoindentation. Appl Surf Sci 2005;252:1915–33. https://doi.org/10.1016/j.apsusc.2005.08.090.
[54] Moeller G. AFM nanoindentation of viscoelastic materials with large end-radius probes. J Polym Sci Pol Phys 2009;47:1573–87.
[55] Nair SS, Wang C, Wynne KJ. AFM peakforce QNM mode for measurement of nanosurface mechanical properties of Pt-cured silicones. Prog Org Coat 2019;126:119–28. https://doi.org/10.1016/j.porgcoat.2018.10.008.
[56] VanLandingham MR, Villarrubia JS, Guthrie WF, Meyers GF. Nanoindentation of polymers: an overview. Macromol Symp 2001;167:15–44.
[57] Dokukin ME, Sokolov I. On the measurements of rigidity modulus of soft materials in nanoindentation experiments at small depth. Macromolecules 2012;45:4277–88. https://doi.org/10.1021/ma202600b.
[58] Eaton P, West P. Atomic Force Microscopy. Oxford, England: Oxford University Press; 2010.
[59] Vande Putte L. Caractérisation mécanique de matériaux souples à plusieurs échelles de mesure différentes. Master's thesis. UCLouvain, 2021.
[60] Myshkin N, Kovalev A, Spaltman D, Woydt M. Contact mechanics and tribology of polymer composites. J Appl Polym Sci 2014;131:39870. https://doi.org/10.1002/app.39870.
[61] Winter B. Linear models and linear mixed effects models in R with linguistic applications 2013.
[62] Gayot SF, Bailly C, Pardoen T, Gérard P. Relationship between processing parameters and mechanical properties of thick glass fibre reinforced thermoplastic methacrylic composites. Proceedings of the 7th ECCOMAS Thematic Conference on the Mechanical Response of Composites, Girona, Spain: A. Turon, P. Maimí, M. Fagerström (ed.); 2019.
[63] Schneider CA, Rasband WS, Eliceiri KW. NIH image to ImageJ: 25 years of image analysis. Nat Methods 2012;9:671–5. https://doi.org/10.1038/nmeth.2089.
[64] Bahrami A, Bailly C, Nysten B. Spatial resolution and property contrast in local mechanical mapping of polymer blends using AFM dynamic force spectroscopy. Polymer 2019;165:180–90. https://doi.org/10.1016/j.polymer.2019.01.023.
[65] Nečas D, Klapetek P. Gwyddion: An open-source software for SPM data analysis. Centr Eur J Phys 2012;10:181–8. https://doi.org/10.2478/s11534-011-0096-2.
[66] R Core Team. R: A Language and Environment for Statistical Computing. Vienna, Austria: R Foundation for Statistical Computing; 2023.
[67] Heinze K, Arnould O, Delenne J-Y, Lullien-Pellerin V, Ramonda M, George M. On the effect of local sample slope during modulus measurements by contact-resonance atomic force microscopy. Ultramicroscopy 2018;194:78–88. https://doi.org/10.1016/j.ultramic.2018.07.009.
[68] Voyiadjis GZ, Peters R. Size effects in nanoindentation: An experimental and analytical study. Acta Mech 2010;211:131–53. https://doi.org/10.1007/s00707-009-0222-z.
[69] Pharr GM, Herbert EG, Gao Y. The indentation size effect: A critical examination of experimental observations and mechanistic interpretations. Annu Rev Mat Res 2010;40:271–92. https://doi.org/10.1146/annurev-matsci-070909-104456.
[70] Tadjiev DR, Hand RJ, Hayes SA. Calibrating a nanoindenter for very shallow depth indentation using equivalent contact radius. Phil Mag 2010;90:1819–32. https://doi.org/10.1080/14786430903571420.
[71] Guillonneau G, Kermouche G, Bec S, Loubet J-L. Extraction of mechanical properties with second harmonic detection for dynamic nanoindentation testing. Exp Mech 2012;52:933–44. https://doi.org/10.1007/s11340-011-9561-5.
[72] Frigione M, Rodríguez-Prieto A. Can accelerated aging procedures predict the long term behavior of polymers exposed to different environments? Polymers (Basel) 2021;13:2688. https://doi.org/10.3390/polym13162688.

Glossary

AFM: atomic force microscopy
CI: confidence interval
CSM: continuous stiffness measurement
DMT: Derjaguin-Muller-Toporov
DSC: differential scanning calorimetry
FE: finite element
IIT: instrumented indentation technique
PF: PeakForce
PFT-QNM: PeakForce Tapping® quantitative nanomechanical mapping
UD: unidirectional
PMMA: poly(methyl methacrylate).